Oxygen-enhanced MRI of the lungs: Intraindividual comparison between 1.5 and 3 Tesla

Sven F. Thieme[1], Olaf Dietrich[2], Daniel Maxien[1], Konstantin Nikolaou[1], Stefan O. Schoenberg[3], Maximilian F. Reiser[1], Christian Fink[3]

[1] Ludwig Maximilian University of Munich, Department of Clinical Radiology – Grosshadern, Munich, Germany

[2] Ludwig Maximilian University of Munich, Josef Lissner Laboratory for Biomedical Imaging, Department of Clinical Radiology – Grosshadern, Munich, Germany

[3] Department of Clinical Radiology and Nuclear Medicine, University Medical Center Mannheim, Medical Faculty Mannheim, University of Heidelberg, Mannheim, Germany

Final version: *RoFo Fortschr Röntgenstr* 2011: **183:** 358–364 <URL:http://dx.doi.org/10.1055/s-0029-1245808>

Abstract

Purpose: To assess the feasibility of oxygen-enhanced MRI of the lung at 3 Tesla and to compare signal characteristics with 1.5 Tesla.

Methods: 13 volunteers underwent oxygen-enhanced lung MRI at 1.5 and 3 T with a T1-weighted single-slice non-selective inversion-recovery single-shot half-Fourier fast-spin-echo sequence with simultaneous respiratory and cardiac triggering in coronal orientation. 40 measurements were acquired during room air breathing and subsequently during oxygen breathing (15 L/min, close-fitting face-mask). The signal-to-noise ratio (SNR) of lung tissue was determined with a difference image method. Image quality of all acquisitions was visually assessed. Mean values of the oxygen-induced relative signal enhancement and its regional coefficient of variation were calculated and the signal enhancement was displayed as color-coded parameter maps. Oxygen-enhancement maps were visually assessed with respect to distribution and heterogeneity of the oxygen-related signal enhancement at both field strengths.

Results: The mean relative signal enhancement due to oxygen breathing was 13% (±5.6%) at 1.5 T and of 9.0% (±8.0%) at 3 T. The regional coefficient of variation was significantly higher at 3 T. Visual and quantitative assessment of the enhancement maps showed a considerably less homogeneous distribution of the signal enhancement at 3 T. The SNR was not significantly different but showed a trend to slightly higher values (about 10% increase) at 3 T.

Conclusion: Oxygen-enhanced pulmonary MRI is feasible at 3 Tesla. However, signal enhancement is currently more heterogeneous and slightly lower at 3 T.

Key words:

3 Tesla MRI; Oxygen-enhanced lung MRI; Lung MRI

Corresponding Author:

PD Dr. Olaf Dietrich
Josef Lissner Laboratory for Biomedical Imaging
Institut für Klinische Radiologie
Ludwig-Maximilians-Universität München
Klinikum Großhadern
Marchioninistr. 15
81377 München
Tel: +49-89-7095-4622
Fax: +49-89-7095-4627
od@dtrx.net

Introduction

Gas exchange of oxygen and carbon dioxide is the primary and most important function of the lung. There are several individual components of gas exchange, which can be affected in lung disease. For example, ventilation of the alveoli is disturbed in airway disease such as asthma or chronic obstructive pulmonary disease, which causes decreased oxygen delivery to the alveoli. Diffusion of gases between the alveoli and pulmonary capillaries is disturbed, e.g., in interstitial lung disease. Finally, lung perfusion is required for gas exchange and may be affected in pulmonary vascular disease such as pulmonary embolism.

Oxygen-enhanced magnetic resonance imaging (MRI) of the lungs allows a non-invasive regional visualization of lung function and gas exchange without ionizing radiation. Following diffusion from the alveoli into the capillaries, molecular oxygen acts as a weakly paramagnetic and T1-shortening MR contrast agent and can be used to visualize ventilated lung with functioning oxygen transfer and perfusion (1-6). A major drawback of oxygen-enhanced MRI is the very limited signal-to-noise ratio (SNR) resulting from the low proton-density and the short T2* relaxation time of the lungs. As a consequence, usually multiple averages are required to visualize the small signal differences observed between inhalation of oxygen and room-air, which results in a long acquisition time of oxygen-enhanced MRI (7).

Recently, high-field 3-Tesla MRI has become clinically available. Theoretically, 3-T MRI offers an approximately doubled SNR compared to 1.5 T. On the other hand, for lung MRI, susceptibility effects caused by the large number of air-tissue interfaces within the lungs are increased at 3 T and must be expected to reduce the SNR (8, 9). Up to now, the quantitative effect of high magnetic fields on signal quality in the lung parenchyma and on signal changes caused by oxygen breathing has not yet been examined.

Therefore, the aim of this study was to assess the feasibility of oxygen-enhanced MRI at 3 T and to intraindividually compare the signal characteristics with 1.5 T.

Materials and Methods

Subjects

The study population included 13 non-smoking volunteers (6 men, 7 women), median age 31 years (19 to 55 years). None of them had any known disease of the respiratory or cardiac system. Ethics committee approval was obtained, and all volunteers gave written informed consent before investigation.

Oxygen-enhanced imaging

All exams were performed on two whole-body MRI systems with field strengths of 1.5 and 3 Tesla (Magnetom Avanto and Magnetom Trio, Siemens Healthcare, Erlangen, Germany). Both systems were equipped with 32 independent receiver channels and a 45-mT/m gradient system. Measurements were performed using 9 elements of the integrated spine array coils in combination with a six-element phased-array body matrix coil.

Because many patients with lung diseases will be unable to breath hold long enough to enable breath-hold imaging techniques, and considering the altered pulmonary physiology due to breath holding (3), similar to previous studies (10, 11) we implemented a free-breathing acquisition technique. In order to minimize cardiac and respiratory motion artifacts a double respiratory and cardiac triggering method was used (12) with a navigator acquisition for the monitoring of diaphragm motion and ECG monitoring, as described elsewhere (10). This double triggering was realised by the commercially available 2D prospective acquisition correction (PACE) software (Siemens Healthcare, Erlangen, Germany) and is based on the ECG signal and on the real-time acquisition of one-dimensional image data through the diaphragm (spatially resolved in head-foot direction) to monitor the current diaphragm position and to trigger the image acquisition. Thus, image acquisition should be confined to comparable time points within the cardiac and respiratory cycle.

All subjects were supplied with an MR compatible oxygen mask with an additional 1-liter reservoir bag. According to a recent study, a closed O_2-delivering system was not used, offering no advantage over conventional face masks (13). The mask was plugged to an oxygen outlet in the examination room and was fitted to the subjects before

they entered the scanner in a supine position. Since gravity influences the lung tissue density, the lung signal intensity is increased in lower pulmonary regions, i.e. in the posterior lung portions in supine position (14). Therefore, one coronal slice at the level of the descending aorta was defined as reference level for image acquisition in each examination to assure comparability. A T1-weighting single-slice non-selective inversion-recovery (IR) half-Fourier-acquisition single-shot turbo-spin-echo (HASTE) sequence (15) in coronal orientation was positioned at this level. The following optimized imaging parameters were used at both field strengths: TI=1300 ms; TR=1 respiratory cycle; TE=16 ms; FOV=500×500 mm²; matrix size=128×128; slice thickness=20 mm.

Scanning was initiated with the consecutive acquisition of 40 identically located coronal slices at the breathing of room air. Afterwards, an oxygen flow of 15 L/min, which has been shown to be the optimal flow rate for this imaging method (16), was applied to the mask. A delay of 3 minutes was allowed for the washing in of oxygen into the alveoli, saturation of oxygen concentration, and for diffusion into the pulmonary capillaries. Finally, another 40 data sets were acquired at the same anatomical position during continuous oxygen breathing.

Image postprocessing and data analysis

Motion correction and vessel removal

As a first step of post-processing, a retrospective motion correction was performed as described in detail elsewhere (7). The vertical diaphragm position in all repetitions was compared with the diaphragm position in an average image, and only acquisitions with identical diaphragm position within 3 pixels were accepted for further processing to avoid signal intensity changes (17). The fraction of accepted acquisitions (of all 40 room air and 40 oxygen acquisitions) was determined to describe the technical success rate of each measurement, and was statistically compared between 1.5 and 3 T as well as between oxygen and room air application. Then, the lungs were segmented manually by defining two regions of interest (right and left lung) with a distance of at least 5 mm to surrounding structures such as the diaphragm or central pulmonary vessels. To reduce the influence of the increased signal intensity in smaller pulmonary vessels and to focus the following evaluation to the effects in lung parenchyma, we calculated a mask that excludes those 30% of all pixels in the segmented regions that had the highest signal intensities in a maximum-intensity projection over all acquisitions.

Determination of SNR in lung parenchyma

The measurement of the image noise level was based on difference images since, frequently, artifact-free background regions for noise measurements were not available (the acquisitions contained background regions only in phase-encoding direction, i.e. left or right from the thorax or neck, which were superposed by signal blurring and ghosting artifacts); in addition, the noise level was not uniform over the image due to the application of a distortion-correction ("large field-of-view") filter and an intensity-normalization filter (18).

A small circular region (52 pixels) was defined in an artifact-free area of the right or left upper lung. 39 difference images (calculated from all pairs of consecutive acquisitions) were evaluated (separately for both the air and the oxygen scans) by determining the standard deviation of the difference signal in the circular region (after removal of those pixels that belong to small vessels according to the vessel mask). Of these 39 data sets we then chose those 5 with the smallest standard deviation, i.e. with fewest non-noise artifacts in the selected region (see Fig. 1); the noise level was finally calculated from these 5 regions as the standard deviation divided by the square root of 2.

The signal intensity of the lung tissue was defined as the mean value of the image signal in the same region averaged over all considered acquisitions, and the final SNR was then calculated as the quotient of signal intensity and noise level.

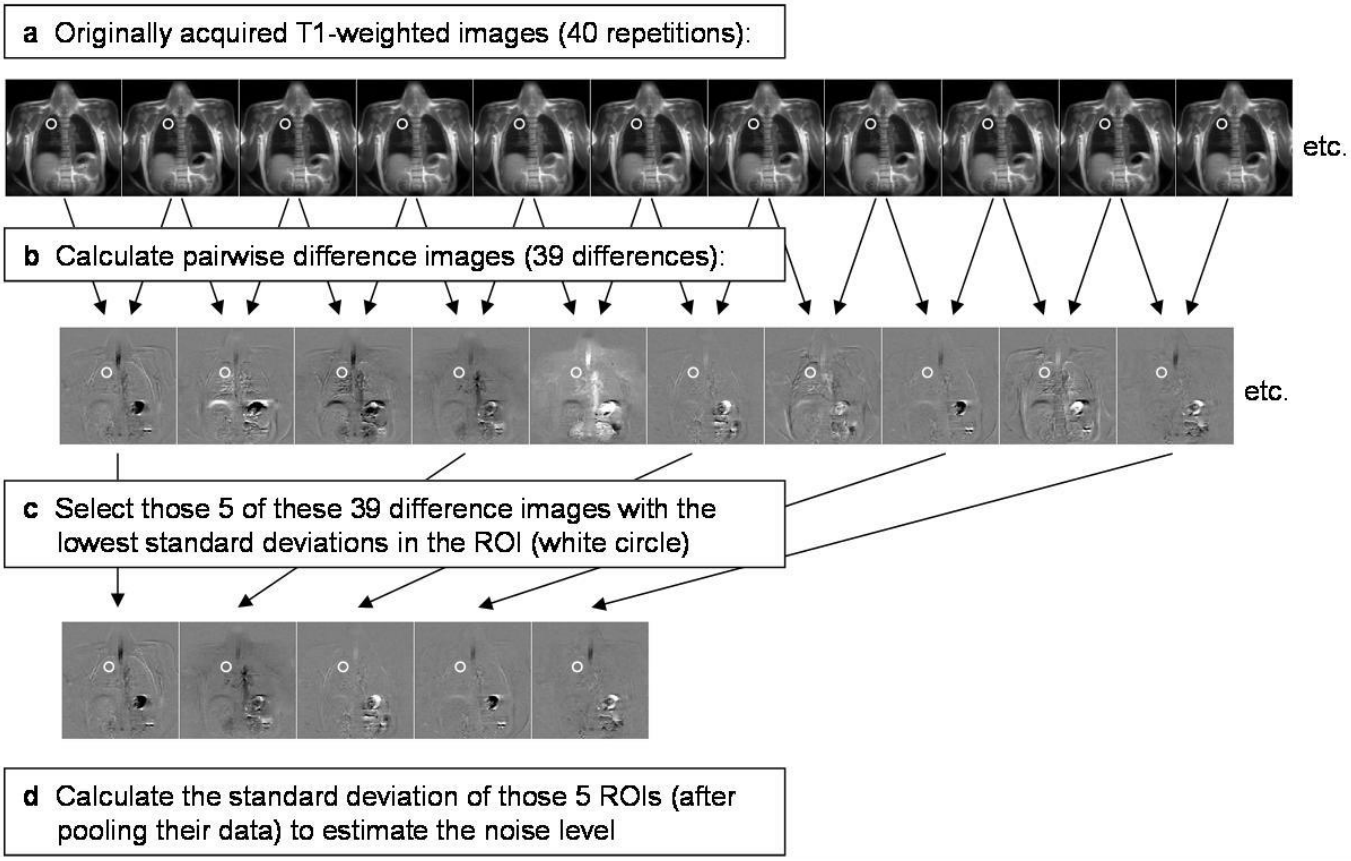

Figure 1: Estimation of noise and SNR in T1-weighted lung images. (a) The originally acquired image data (40 repetitions) with the region of interest (ROI, white circle) in the upper lung. (b) Difference images calculated by pairwise subtraction of subsequently acquired repetitions. The standard deviation in the ROI does not only reflect pure noise but also artifacts due to motion (e.g., different diaphragm or stomach positions and blood pulsation), which increase the standard deviation. (c) To minimize the influence of these artifacts, we selected those 5 difference images with minimal standard deviation in the ROI. (d) The noise level was estimated as the standard deviation of the pooled pixel intensities of the 5 remaining ROIs divided by the square root of 2.

Evaluation of oxygen enhancement, enhancement maps

All accepted images of room air measurements on the one hand and of oxygen measurements on the other hand were averaged, and a map of relative signal increase $\Delta S_{rel} = (S_{oxygen}-S_{air})/S_{air}$ was calculated. To reduce the influence of statistical noise, the maps were low-pass filtered before visualization using a 3×3 Gauss filter with a standard deviation of 1 pixel. The mean value of the relative signal enhancement over the segmented lung was calculated as measure of the oxygen-induced signal enhancement. The regional coefficient of variation (or relative dispersion), i.e., the regional standard deviation of the relative signal enhancement over the segmented lung divided by the mean value was calculated to assess the heterogeneity of the signal enhancement within the lung (19, 20).

All acquisitions were visually assessed by two radiologists with regard to image quality (acceptable / not acceptable). Oxygen enhancement maps were visually assessed by the same two readers in consensus and were compared intraindividually regarding the distribution and heterogeneity of the oxygen-related signal enhancement at 1.5 T and 3 T.

Statistical analysis

The Wilcoxon Matched-Pairs Signed-Ranks Test was used for comparison of SNRs, motion-correction results, oxygen enhancement, and the regional coefficient of variation of the enhancement at 1.5 and 3 Tesla. The same test was used to compare SNRs and motion-correction results between acquisitions during breathing of room air and oxygen. A p value < 0.05 was considered statistically significant.

Results

All examinations were completed without complications and with acceptable image quality; examples

of the acquired T1-weighted images are shown in Fig. 2.

As a result of the retrospective motion correction based on the diaphragm position, a significantly higher fraction of accepted acquisitions was found at 1.5 Tesla (mean value of accepted images averaged over all volunteers 95%, standard deviation (SD) 6.7%) than at 3 Tesla (83% accepted, SD 18%, $p<.05$). Both at 1.5 and 3 T, there was no statistically significant difference between the percentage of accepted measurements at room air and during oxygen breathing.

The SNR based on measurements in the small region of interest (ROI) in the upper lungs was slightly higher (by about 10%) at 3 T compared to 1.5 T, both at room air and during oxygen breathing (see Table 1). However, these differences did not show statistical significance. As an effect of oxygen-induced T1-shortening, SNR in the small ROI was slightly higher in the oxygen acquisitions, compared to the room air measurements; again, these differences were not statistically significant.

In the segmented lungs, the mean relative signal enhancement due to oxygen breathing was 13% (SD 5.6%) at 1.5 Tesla and 9.0% (SD 8.0%) at 3 Tesla (see Table 2). Even though there was a trend towards a higher signal enhancement at a field strength of 1.5 Tesla, those values were not statistically significantly different compared to 3 Tesla. However, the regional coefficient of variation of the relative signal enhancement as a measure for its heterogeneity was significantly higher at 3.0 Tesla ($p<.05$) than at 1.5 Tesla. The visual assessment of the enhancement maps supported this result with a considerably more homogenous distribution of the pulmonary parenchymal signal enhancement at 1.5 Tesla (see Fig. 3).

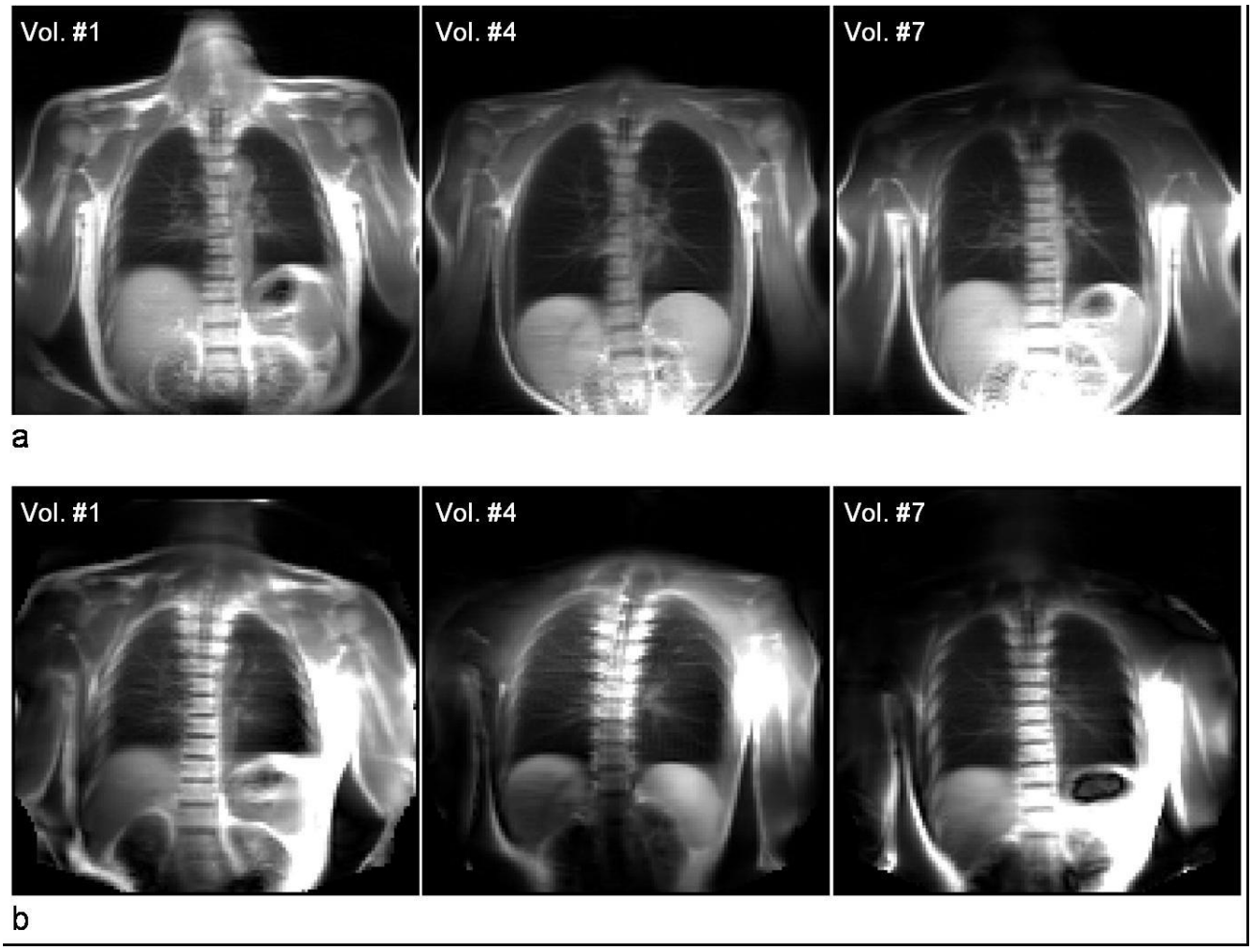

Figure 2: Examples of T1-weighted images of 3 volunteers breathing pure oxygen acquired at (a) 1.5 Tesla and (b) 3 Tesla. Note the substantial non-uniformities of the signal intensities at 3 Tesla.

Table 1: Signal-to-noise ratio of lung tissue in T1-weighted acquisitions

	1.5 Tesla Signal-to-noise ratio		3 Tesla Signal-to-noise ratio	
	Room air	Oxygen	Room air	Oxygen
Mean value	68.7	71.0	76.5	82.6
Std. dev.	18.6	21.6	31.1	32.1

Table 2: Oxygen-induced relative signal enhancement of lung tissue at 1.5 and 3 Tesla

	1.5 Tesla Relative signal enhancement (%)		3 Tesla Relative signal enhancement (%)	
	Mean value	Regional CV (heterogeneity)	Mean value	Regional CV (heterogeneity)
Volunteer #1	10.1	76.8	7.9	148.2
Volunteer #2	10.5	46.2	4.0	156.4
Volunteer #3	22.4	23.6	1.8	494.9
Volunteer #4	13.6	57.0	9.3	94.5
Volunteer #5	17.8	31.7	4.5	111.2
Volunteer #6	10.2	37.5	1.8	324.7
Volunteer #7	17.7	32.8	23.2	73.1
Volunteer #8	21.8	49.2	27.3	58.4
Volunteer #9	8.2	73.2	14.2	109.0
Volunteer #10	10.9	32.6	4.4	102.9
Volunteer #11	3.0	171.3	8.0	75.3
Volunteer #12	8.9	60.2	4.2	114.1
Volunteer #13	14.5	72.2	6.2	152.5
Mean value	**13.0**	**58.8***	**9.0**	**155.0***
Std. dev.	**5.6**	**38.1**	**8.0**	**122.1**

* values with statistically significant difference comparing 1.5 T and 3 T ($p<0.05$, Wilcoxon matched-pairs signed-ranks test)

CV: coefficient of variation

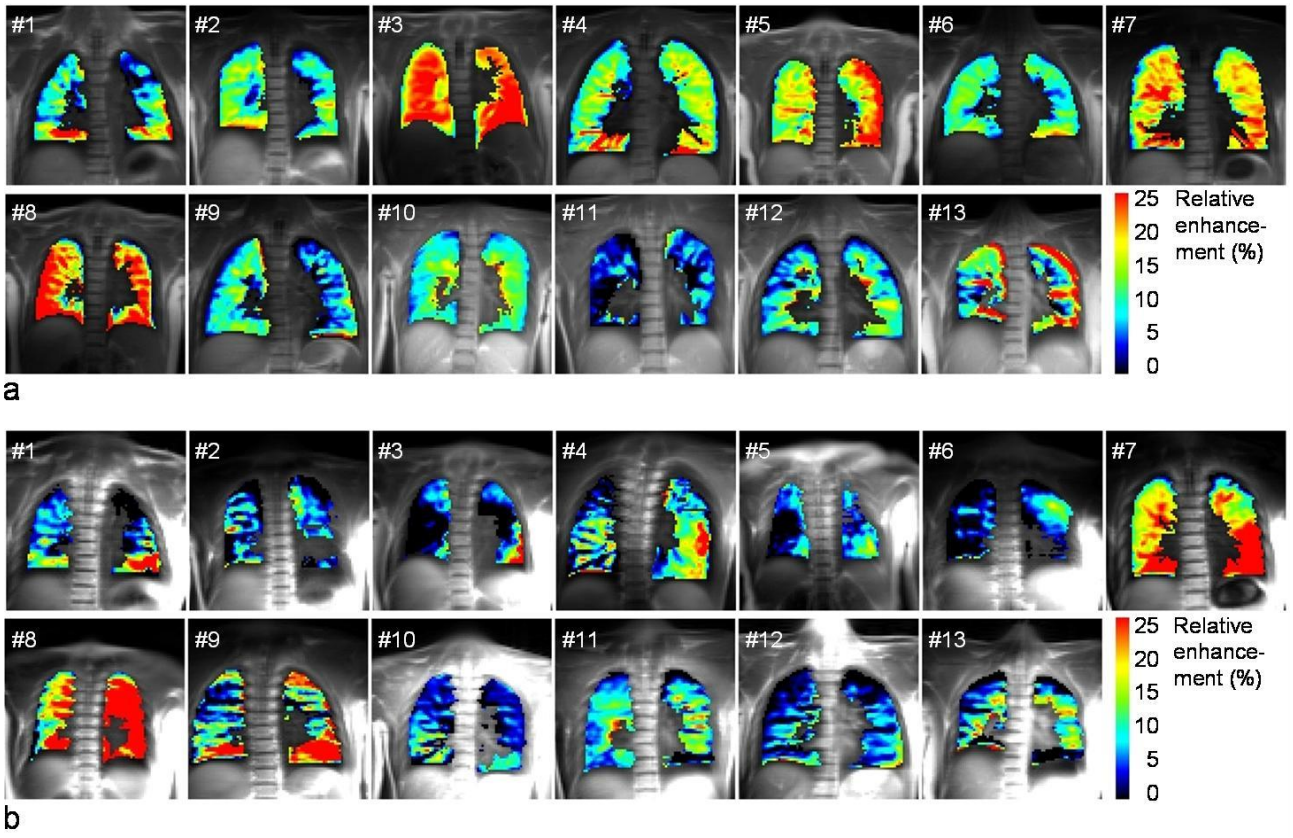

Figure 3: Signal-enhancement maps of all 13 volunteers acquired at (a) 1.5 Tesla and (b) 3 Tesla. Note the slightly lower oxygen-induced signal enhancements and the substantially higher heterogeneity of the enhancement at 3 Tesla.

Discussion

Although in the recent years pulmonary MRI has emerged as an alternative imaging tool for various lung pathologies without patient exposure to ionizing radiation and has been subject to continuous improvements in acquisition techniques including dynamic measurements (21-24), high-field MRI of the lungs at a field strength of 3 Tesla or higher is in a rather experimental stage up to now. In clinical routine of pulmonary examinations, this technique is subordinate to pulmonary MRI at 1.5 T. Using an intraindividual approach, Fink et al. compared five different pulse sequences at 1.5 and 3 Tesla regarding image quality and lesion contrast and demonstrated a comparable image quality as well as a higher lesion contrast at 3 T (9). Compared to 1.5 T, Nael et al. found an increased SNR in the pulmonary vasculature at 3 T, when performing contrast-enhanced pulmonary MR angiography (however, with a lower parenchymal enhancement in perfusion MRI) (25, 26). In our opinion, these initial results are insinuating a potential role for high-field pulmonary MRI in the future.

In pulmonary functional imaging, oxygen-enhanced MRI has emerged as a diagnostic tool for the regional assessment of the pulmonary function (i.e., ventilation, diffusion, and parenchymal perfusion) (1-4, 27, 28). Thus, in patients with pulmonary functional impairment, oxygen-enhanced MR imaging can be part of the diagnostic procedure. However, up to now, this method has not been systematically investigated at higher magnetic field strengths than 1.5 T. With regard to the potential advantages of high-field MRI, e.g. in pulmonary MR angiography, and thinking of a potentially integrated MR imaging concept, e.g. combination of pulmonary MR angiography and oxygen-enhanced imaging, the feasibility and the potential advantages of oxygen-enhanced MRI at 3 Tesla need to be further investigated.

The sequence type used in this study is a T1-weighting single-shot inversion-recovery turbo spin echo (or fast spin echo) sequence, which was demonstrated to be well suited for oxygen-enhanced imaging in many previous studies, leading to a measurable signal increase due to inhaled oxygen (1, 4, 7, 10, 16, 29-31) In addition, in a study comparing five different pulse sequences in

volunteers and in a porcine model at 1.5 and 3 T, this type of sequence has been shown to have similar imaging characteristics in pulmonary MRI at both field strengths and to be superior to all other tested sequences for assessment of the pulmonary parenchyma at 3 T (9). In this study, we chose identical imaging parameters at 1.5 and 3 T based on the observation that there are no relevant differences in relaxation parameters at both field strengths. In particular, we used the same inversion time of 1300 ms at 1.5 and 3 Tesla since first results indicate that the T1 relaxation time of lung tissue at both field strengths is relatively similar: Breathing room air, typical T1 values at 1.5 Tesla were found in the range between about 1200 and 1400 ms (16, 30-32), although some early studies observed shorter relaxation times of about 900 ms (1, 29). At 3 Tesla, Nichols and Paschal recently reported a T1 of (1374±226) ms (33); preliminary oxygen-enhanced measurements at 3 Tesla resulted in T1 values of 1281 ms and 1102 ms when breathing room air and pure oxygen, respectively (34). Since there is no clear trend towards longer T1 relaxation times at 3 Tesla compared to 1.5 Tesla, it appeared reasonable to choose the same optimal inversion time (30) for both field strengths. The echo time was chosen as short as possible at both field strengths to minimize the T2-weighting of the sequence.

Our SNR measurements could not show a significant SNR difference for the 3 T acquisitions compared to 1.5 T. A theoretically achievable doubling of the SNR as a consequence of the doubling in the magnetic field strength might be partially antagonized by increasing magnetic susceptibility effects of pulmonary structures due to their microscopic heterogeneity. However, our measurements in 13 volunteers demonstrated a certain (not statistically significant) SNR increase due to oxygen resulting in a measurable relative pulmonary signal enhancement at 3 T. These results indicate that there might be a potential for an application of this functional pulmonary imaging method in high-field MRI.

Our quantitative results as well as the visual inspection of the enhancement maps reveal an inferior image quality of the examinations at 3 T with a significantly higher heterogeneity of the signal enhancement. In our opinion, the predominant factor responsible for this relatively poor performance at 3 Tesla is the lower B1 homogeneity: The well-known B1 (or flip angle) inhomogeneity at 3 Tesla (35) results in a partially imperfect inversion and, thus, in very different T1-weighting in different areas of the lungs. However, sufficient oxygen-induced signal enhancement can only be obtained after a complete and homogeneous inversion of the magnetization. In addition, the signal quality is reduced by imperfect 180° refocusing pulses at 3 Tesla.

The intraindividual comparison of the enhancement maps at 1.5 and 3 T clearly shows that 3-T images are currently not fully suited for the assessment of pulmonary functional parameters, as the heterogeneity of the signal enhancement could simulate pathologies in healthy subjects who do not show any abnormalities with a rather homogeneous enhancement in the 1.5-T maps. In order to improve the image quality, several different approaches are possible: The general B1 homogeneity of the MRI system could be further improved, e.g. by employing advanced excitation techniques such as RF shimming and parallel-transmit approaches. In addition, more robust inversion pulses might be applied that (at least partially) compensate for B1 inhomogeneities (36). In the present study, however, we decided to apply the same (default) inversion pulse available for single-shot TSE imaging at both used MRI systems since optimizing the inversion properties at 3 Tesla was beyond the scope of the study. As a further alternative, it might be advantageous to use a saturation-recovery instead of an inversion-recovery preparation at 3 Tesla, since the former is intrinsically less sensitive to B1 inhomogeneities.

We did not find a fully satisfying explanation for the differences between 1.5 and 3 Tesla with respect to the retrospective motion correction. Possibly, the edge detecting algorithm failed in some cases at 3-T acquisitions because of B1-related signal voids in the region of the diaphragm. Another explanation might be that the ECG triggering was less efficient at 3 T because of the magnetohydrodynamic effect (35) and, thus, the actual cardiac triggering of the acquisition might have been delayed such that the acquisition no longer fit into the end-expiration period.

Conclusion

Our intraindividual comparison demonstrated that oxygen-enhanced magnetic resonance imaging is generally feasible at a field strength of 3 Tesla, implying a potential for this imaging technique at higher magnetic fields. However, using identical acquisition techniques and imaging parameters at both field strengths, the obtained image quality of the oxygen maps was considerably inferior at 3 Tesla than at 1.5 Tesla due to a significantly higher heterogeneity of the signal enhancement. Thus, further optimizations such as improved B1 uniformity and more robust inversion pulses are required to finally allow an effective integration of oxygen-enhanced MRI in comprehensive pulmonary MRI protocols at 3 Tesla.

References

1. Edelman RR, Hatabu H, Tadamura E, Li W, Prasad PV. Noninvasive assessment of regional ventilation in the human lung using oxygen-enhanced magnetic resonance imaging. Nat Med. 1996;2(11):1236-9.
2. Ohno Y, Chen Q, Hatabu H. Oxygen-enhanced magnetic resonance ventilation imaging of lung. Eur J Radiol. 2001;37(3):164-71.
3. Ohno Y, Hatabu H. Basics concepts and clinical applications of oxygen-enhanced MR imaging. Eur J Radiol. 2007;64(3):320-8.
4. Muller CJ, Schwaiblmair M, Scheidler J, et al. Pulmonary diffusing capacity: assessment with oxygen-enhanced lung MR imaging preliminary findings. Radiology. 2002;222(2):499-506.
5. Nakagawa T, Sakuma H, Murashima S, Ishida N, Matsumura K, Takeda K. Pulmonary ventilation-perfusion MR imaging in clinical patients. J Magn Reson Imaging. 2001;14(4):419-24.
6. Arnold JF, Kotas M, Fidler F, Pracht ED, Flentje M, Jakob PM. Quantitative regional oxygen transfer imaging of the human lung. J Magn Reson Imaging. 2007;26(3):637-45.
7. Dietrich O, Losert C, Attenberger U, et al. Fast oxygen-enhanced multislice imaging of the lung using parallel acquisition techniques. Magn Reson Med. 2005;53(6):1317-25.
8. Bergin CJ, Glover GH, Pauly JM. Lung parenchyma: magnetic susceptibility in MR imaging. Radiology. 1991;180(3):845-8.
9. Fink C, Puderbach M, Biederer J, et al. Lung MRI at 1.5 and 3 Tesla: observer preference study and lesion contrast using five different pulse sequences. Investigative radiology. 2007;42(6):377-83.
10. Molinari F, Eichinger M, Risse F, et al. Navigator-triggered oxygen-enhanced MRI with simultaneous cardiac and respiratory synchronization for the assessment of interstitial lung disease. J Magn Reson Imaging. 2007;26(6):1523-9.
11. Molinari F, Gaudino S, Fink C, et al. Simultaneous cardiac and respiratory synchronization in oxygen-enhanced magnetic resonance imaging of the lung using a pneumotachograph for respiratory monitoring. Investigative radiology. 2006;41(5):476-85.
12. Vaninbroukx J, Bosmans H, Sunaert S, et al. The use of ECG and respiratory triggering to improve the sensitivity of oxygen-enhanced proton MRI of lung ventilation. European radiology. 2003;13(6):1260-5.
13. Molinari F, Puderbach M, Eichinger M, et al. Oxygen-enhanced magnetic resonance imaging: influence of different gas delivery methods on the T1-changes of the lungs. Investigative radiology. 2008;43(6):427-32.
14. Prisk GK, Yamada K, Henderson AC, et al. Pulmonary perfusion in the prone and supine postures in the normal human lung. J Appl Physiol. 2007;103(3):883-94.
15. Ohno Y, Oshio K, Uematsu H, Nakatsu M, Gefter WB, Hatabu H. Single-shot half-Fourier RARE sequence with ultra-short inter-echo spacing for lung imaging. J Magn Reson Imaging. 2004;20(2):336-9.
16. Mai VM, Liu B, Li W, et al. Influence of oxygen flow rate on signal and T(1) changes in oxygen-enhanced ventilation imaging. J Magn Reson Imaging. 2002;16(1):37-41.
17. Bankier AA, O'Donnell CR, Mai VM, et al. Impact of lung volume on MR signal intensity changes of the lung parenchyma. J Magn Reson Imaging. 2004;20(6):961-6.
18. Dietrich O, Raya JG, Reeder SB, Reiser MF, Schoenberg SO. Measurement of signal-to-noise ratios in MR images: influence of multichannel coils, parallel imaging, and reconstruction filters. J Magn Reson Imaging. 2007;26(2):375-85.
19. Dehnert C, Risse F, Ley S, et al. Magnetic resonance imaging of uneven pulmonary perfusion in hypoxia in humans. American journal of respiratory and critical care medicine. 2006;174(10):1132-8.
20. Levin DL, Buxton RB, Spiess JP, Arai T, Balouch J, Hopkins SR. Effects of age on pulmonary perfusion heterogeneity measured by magnetic resonance imaging. J Appl Physiol. 2007;102(5):2064-70.
21. Hintze C, Stemmer A, Bock M, et al. A hybrid breath hold and continued respiration-triggered technique for time-resolved 3D MRI perfusion studies in lung cancer. Rofo. 2010;182(1):45-52.
22. Ley-Zaporozhan J, Ley S, Sommerburg O, Komm N, Muller FM, Schenk JP. Clinical application of MRI in children for the assessment of pulmonary diseases. Rofo. 2009;181(5):419-32.
23. Tetzlaff R, Eichinger M, Schobinger M, Puderbach M, Meinzer HP, Kauczor HU. Semiautomatic assessment of respiratory motion in dynamic MRI--comparison with simultaneously acquired spirometry. Rofo. 2008;180(11):961-7.
24. Wolf T, Anjorin A, Posselt H, Smaczny C, Vogl TJ, Abolmaali N. MRT-basierte Flussmessungen im Truncus pulmonalis zur Detektion einer pulmonal-arteriellen Hypertonie in Patienten mit zystischer Fibrose. Rofo. 2009;181(2):139-46.
25. Nael K, Michaely HJ, Lee M, Goldin J, Laub G, Finn JP. Dynamic pulmonary perfusion and flow quantification with MR imaging, 3.0T vs. 1.5T: initial results. J Magn Reson Imaging. 2006;24(2):333-9.
26. Nael K, Saleh R, Nyborg GK, et al. Pulmonary MR perfusion at 3.0 Tesla using a blood pool contrast agent: Initial results in a swine model. J Magn Reson Imaging. 2007;25(1):66-72.
27. Ohno Y, Koyama H, Nogami M, et al. Dynamic oxygen-enhanced MRI versus quantitative CT: pulmonary functional loss assessment and clinical stage classification of smoking-related COPD. AJR Am J Roentgenol. 2008;190(2):W93-9.
28. Ohno Y, Iwasawa T, Seo JB, et al. Oxygen-enhanced magnetic resonance imaging versus computed tomography: multicenter study for clinical stage classification of smoking-related chronic obstructive pulmonary disease. American journal of respiratory and critical care medicine. 2008;177(10):1095-102.

29. Stock KW, Chen Q, Morrin M, Hatabu H, Edelman RR. Oxygen-enhanced magnetic resonance ventilation imaging of the human lung at 0.2 and 1.5 T. J Magn Reson Imaging. 1999;9(6):838-41.
30. Loffler R, Muller CJ, Peller M, et al. Optimization and evaluation of the signal intensity change in multisection oxygen-enhanced MR lung imaging. Magn Reson Med. 2000;43(6):860-6.
31. Chen Q, Jakob PM, Griswold MA, Levin DL, Hatabu H, Edelman RR. Oxygen enhanced MR ventilation imaging of the lung. MAGMA Magn Reson Mater Phy. 1998;7(3):153-61.
32. Jakob PM, Hillenbrand CM, Wang T, Schultz G, Hahn D, Haase A. Rapid quantitative lung (1)H T(1) mapping. J Magn Reson Imaging. 2001;14(6):795-9.
33. Nichols MB, Paschal CB. Measurement of longitudinal (T1) relaxation in the human lung at 3.0 Tesla with tissue-based and regional gradient analyses. J Magn Reson Imaging. 2008;27(1):224-8.
34. Dietrich O, Raya JG, Fasol U, Peller M, Reiser MF, Schoenberg SO. Oxygen-enhanced MRI of the lung at 3 Tesla: Feasibility and T1 relaxation times. Proceedings of the International Society for Magnetic Resonance in Medicine (ISMRM) 2006;14:1307.
35. Dietrich O, Reiser MF, Schoenberg SO. Artifacts in 3-T MRI: physical background and reduction strategies. Eur J Radiol. 2008;65(1):29-35.
36. Puderbach M, Ohno Y, Kawamitsu H, et al. Influence of inversion pulse type in assessing lung-oxygen-enhancement by centrically-reordered non-slice-selective inversion-recovery half-Fourier single-shot turbo spin-echo (HASTE) sequence. J Magn Reson Imaging. 2007;26(4):1133-8.

Zusammenfassung

Ziel: Die Machbarkeit der sauerstoffverstärkten MRT der Lunge bei 3 Tesla sollte beurteilt und die Signalcharakteristika mit 1,5 Tesla verglichen werden.

Methoden: 13 Probanden unterzogen sich einer sauerstoffverstärkten MRT-Untersuchung bei 1,5 und 3 T mit einer koronal orientierten T1-gewichteten, einschichtigen, nichtselektiven Inversion-Recovery-Half-Fourier-Fast-Spin-Echo-Sequenz mit Atem- und EKG-Triggerung. Je 40 Einzelmessungen wurden unter Raumluftatmung und unter Sauerstoffatmung (15 L/min über eine Atemmaske) durchgeführt. Das Signal-Rausch-Verhältnis (SNR) von Lungengewebe wurde mithilfe eines Differenzbildverfahrens ermittelt. Die Bildqualität der Einzelakquisitionen wurde visuell beurteilt. Der Mittelwert des sauerstoffvermittelten relativen Signalanstiegs und sein regionaler Variationskoeffizient wurden berechnet und der Signalanstieg in Parameterkarten farbcodiert dargestellt. Verteilung und Heterogenität des Signalanstiegs in den Parameterkarten bei beiden Feldstärken wurden visuell verglichen.

Ergebnisse: Der mittlere relative Signalanstieg durch Sauerstoffatmung betrug 13% (±5.6%) bei 1,5 T und 9.0% (±8.0%) bei 3 T. Ein signifikant höherer Wert des regionalen Variationskoeffizienten zeigte sich bei 3 T. Auf den Parameterkarten zeigte sich visuell und quantitativ bei 3 T eine deutlich inhomogenere Verteilung des Signalanstiegs. Das SNR unterschied sich bei den beiden Feldstärken nicht signifikant, war jedoch bei 3 T tendenziell (um ca. 10%) höher.

Schlußfolgerung: Die sauerstoffverstärkte MRT-Bildgebung der Lunge läßt sich prinzipiell bei 3 T durchführen, wenngleich der Signalanstieg bei 3 T derzeit im Vergleich zu 1,5 T heterogener und etwas geringer ist.